

# A Mechanism of Spatter Production from the Viewpoint of the Integral of Specific Current Action

*A model is proposed to quantitatively explain the mechanism of spatter production and the role of waveform parameters*

BY S. K. KANG AND S. J. NA

**ABSTRACT.** Numerous earlier studies have investigated the mechanism of spatter production, and the waveform parameters affecting spatter production, because more procedures are necessary to remove spatter. These studies explain the spatter mechanism qualitatively, but do not clarify it quantitatively. Also, they do not illustrate how waveform parameters influence spatter production.

In this study, the integral of specific current action is introduced to quantitatively explain the mechanism of spatter production. Based on the previous studies, this study proposes a model that suggests there is a constant value of the integral of a specific current action to determine the moment of spatter production. By comparing the spatter calculations with the welding experiments, this model was validated. Simulations were carried out to investigate the influence of the waveform parameters on spatter production. This quantitatively explains the role of the waveform parameters, such as peak current and arc time, in spatter production.

## Introduction

Gas metal arc welding (GMAW) has been widely used in many industries because of its high productivity, but it has several disadvantages such as spatter production. It is necessary to reduce spatter production because more procedures are necessary to remove the spatter after welding. For this purpose, numerous studies have been carried out to investigate the mechanism of spatter production and the role of waveform parameters in this production.

Chen, Sun, and Fan summarized the mechanism of the spatter production in four main points as follows (Ref. 1):

1) Electric explosion. Under the pinch force produced by the peak current, the short circuit bridge shrinks in cross section

and the current density increases further; consequently, the bridge overheats and evaporates, resulting in an explosion.

2) Gas explosion. The oxygen and carbon in the melted metal react with each other in high-temperature zones, which results in explosion of CO gas.

3) Gas impact. The air is heated and expanded by an abrupt arc reinitiation after a short circuit breakage. The melted metal in the weld pool and remaining droplets are blown off by the impact.

4) Momentary short circuit. At the breakage of the very thin short circuit bridge, a small quantity of spatter may be produced. These viewpoints illustrate the mechanism qualitatively, but not quantitatively.

There have been numerous studies investigating the waveform parameters in spatter production. Several regression models have been proposed to estimate arc stability by extracting the waveform parameters from the signal of the welding current and arc voltage (Ref. 2). A statistical model has been developed to quantitatively predict the process stability by applying the relationship between spatter production and waveform parameters in GMAW with a multiple regression analysis (Ref. 3). Also, a study to estimate spatter production was carried out by using an artificial neural network (Ref. 4). In these studies, the parameters had a relationship with the spatter production by using an index or neural network. However, these studies do not explain how these specified parameters quantitatively influenced spatter production.

The peak current was found to be dominant in spatter production (Ref. 5); thus, various methods were investigated to control the peak current before the short circuit breakage occurred. Several studies were completed using GMAW (Refs. 6–8), while others were completed using pulsed arc welding (Refs. 9, 10). But these papers do not clarify the role of the peak current, which quantitatively affects spatter production.

There are a few works in which the electric explosion of wires was investigated as the property of materials. These works show that the electrical explosion of wires is related to the current density in the order of  $10^7$ – $10^8$  A/cm<sup>2</sup> (Refs. 11–14). The integral of a specific current action was introduced to explain the electrical explosion of wire. It was defined using the following equation:

$$h = \int_0^{t_b} \frac{I^2}{A^2} dt \quad (1)$$

where  $t_b$ ,  $I$ , and  $A$  denote the time of burst, current, and sectional area, respectively. In these works, the explosion experiments were carried out for a wire with a diameter of several  $\mu$ m during the time of several  $\mu$ s. When the wire diameter and short circuit time were compared with those of the current study, they were extremely small.

Bennett and Kahl's study showed that the energy introduced into the wire by the moment of explosion is constant for a given metal (Ref. 13). Anderson and Neilson's work has shown that the integral of a specific current action is constant for a given metal, such as copper, nickel, or iron (Ref. 14). The order of the value of  $h$  is about  $10^7$  A<sup>2</sup>s/cm<sup>4</sup>, while the wire diameter and time are similar to those of this study.

The main objective of this study is to explain spatter production from the viewpoint of the integral of a specific current action. Based on previous studies, the model suggested in this study proposes

## KEYWORDS

Spatter Production  
Waveform Parameters  
Peak Current  
Short Circuit Mode  
Arc Time  
Short Circuit Time  
Droplet Length  
Pinch Radius  
Specific Current Action

S. K. KANG is a graduate student and S. J. NA (sjna@kaist.ac.kr) is a professor of the Dept. of Mechanical Engineering, Korea Advanced Institute of Science and Technology, Daejeon, Republic of Korea.

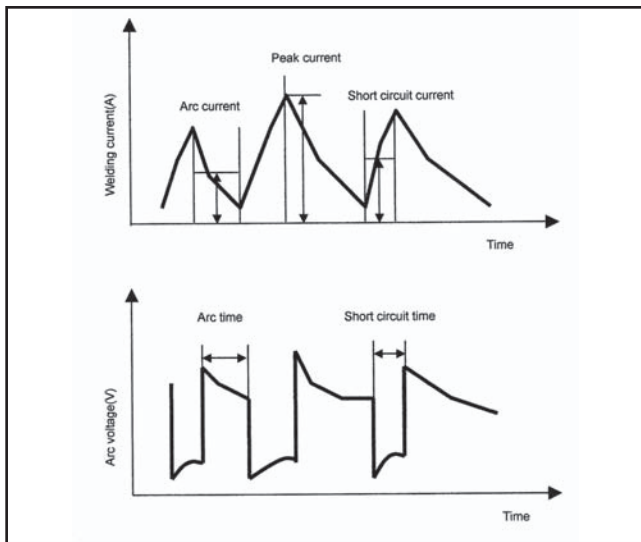


Fig. 1 — Waveforms of welding current and arc voltage in the short circuit mode.

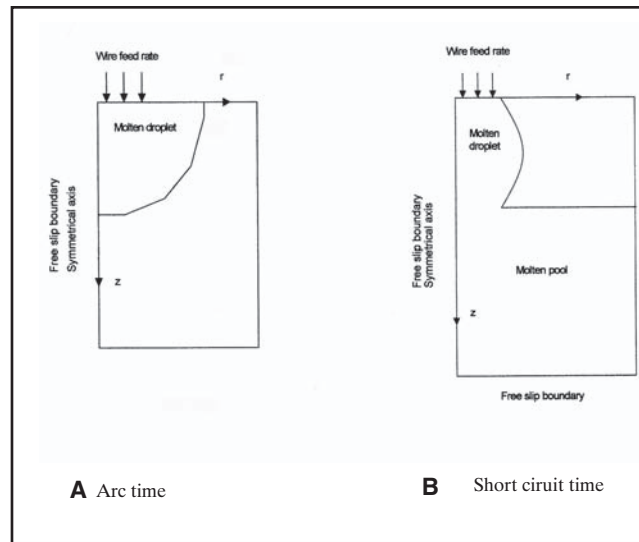


Fig. 2 — Boundary conditions for the simulations in the VOF program.

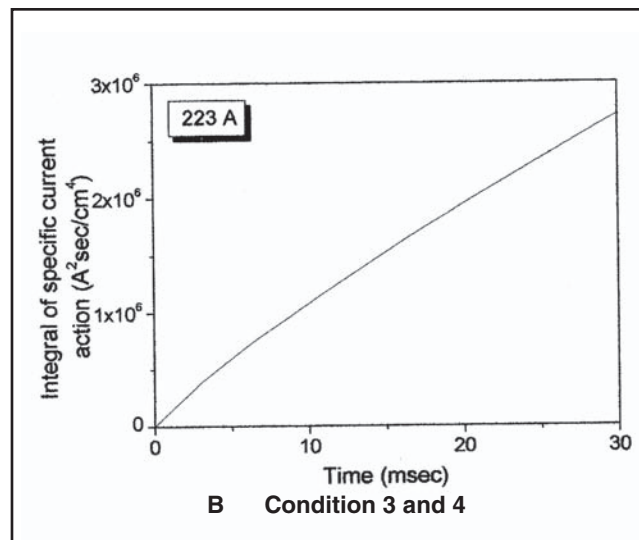
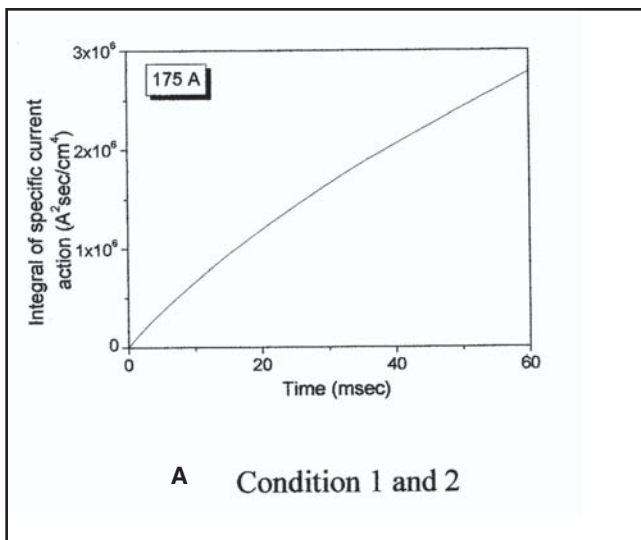


Fig. 3 — Integral of specific current action at the arc time for the conditions in Table 3.

that there is a constant value of  $h$  to determine the moment of a short circuit breakage. To verify this, the related parameters were extracted, and, from the model, spatter production was calculated and compared with the welding experiments.

By using the proposed model, simulations have been carried out to investigate the influence of the droplet volume, arc current, and short circuit current on spatter production. This quantitatively explains the role of the waveform parameters, such as the peak current and arc time, in spatter production.

### Model Description

Based on previous papers, this model is proposed to quantitatively explain spatter production. It has been stated that there is a constant value of  $h$  to determine the mo-

ment of spatter production. To verify this, two steps are necessary — the first is to find the constant value of  $h$ , and the second is to compare the calculated spatter production with the welding experiments to verify the model.

To find the constant value of  $h$ , the procedure and assumption are as follows. From previous GMAW experiments, the majority of the spatter production was found to occur in droplets from the electric explosion and momentary short circuit (Ref. 15). Therefore, it is assumed that spatter production is related to the value of  $h$  across the droplet length, but not with that across the molten pool. Because the short circuit mode is composed of two phases, the arc time and the short circuit time, the values of  $h$  need to be calculated separately. For the arc time, the arc current was used as the simulation

current, and the value of  $h$  was calculated across the droplet and then averaged. For the short circuit time, the peak current was assumed to be the short circuit current and used as the simulation current, because the peak current is dominant in spatter production. The value of  $h$  was calculated in two ways — one way was to calculate and average the value of  $h$  across the total droplet length, and the other was to calculate and average the value of  $h$  at the pinch radius. After calculating the values of  $h$  for the arc time and the short circuit time, the values were summed to find the constant value of  $h$ .

For the spatter calculations, some suitable parameters should be extracted first. Because spatter is directly related to the volume of the short circuit bridge, the parameters affecting this must be considered in the spatter calculations. The fact that

**Table 1 — Welding Variables**

Shielding gas	CO <sub>2</sub> 20% + Ar 80% with a flow rate of 20 L/min
Welding wire	1.2-mm-diameter YGW 15
Welding speed	6 mm/s
CTWD (Contact tube to work distance)	15 mm
Base metal	6-mm-thick ASTM A36M

**Table 2 — Material Properties of Steel**

Mass density	7860 (kg/m <sup>3</sup> )
Kinematic viscosity	2.8 × 10 <sup>-7</sup> (m <sup>2</sup> /s)
Surface tension coefficient	1.8 (N/m)
Electrical conductivity	8.54 × 10 <sup>5</sup> (mho/m)
Permeability	4π × 10 <sup>-7</sup> (H/m)

**Table 3 — Welding Conditions for the Examination of the H-value in Previous Papers**

Condition number	Wire feed rate	Voltage
1	60 mm/s	14.2 V
2	60 mm/s	17.0 V
3	91 mm/s	14.2 V
4	91 mm/s	17.2 V

wire disintegration is related to wire diameter and length was verified experimentally by Nasilowski (Ref. 19). Therefore, it is reasonable to assume that the pinch radius and droplet length at the short circuit breakage affect the spatter generation. Nasilowski's work also showed that the total volume of wire disintegration was influenced by the frequency of droplet. Due to this, the high frequency of the short circuit mode would yield much spatter during a given time. Thus, the pinch radius, the droplet length, and the frequency of the short circuit mode were chosen as the parameters to affect spatter production.

The pinch radius is calculated at the moment of the constant value of h, and is defined as R<sub>total</sub> when the value of h is calculated across the total droplet length, but is defined as R<sub>pinch</sub> when the value of h is calculated at the pinch radius.

The droplet volume plays an important role in determining the droplet length. The droplet is assumed to touch the molten pool with a contact diameter of 1.2

mm (the wire diameter) at the beginning of the short circuit time, which is needed to maintain the simulation stability (Ref. 18). At that time, the ratio of the droplet length to the diameter is assumed to be approximately 1.5, in accordance with pictures from previous welding experiments (Ref. 16). The droplet length was calculated from these assumptions, and the frequency was calculated by the arc time and the short circuit time of the welding experiments. In the latter section of this study, the frequency was calculated by the results of the simulations.

With these calculated parameters, four methods for calculating spatter production are proposed, as shown in Equation 2,

$$\begin{aligned}
 S_1 &= K_1 \cdot f \cdot R_{total} \cdot R_{total} \\
 S_2 &= K_2 \cdot f \cdot R_{pinch} \cdot R_{pinch} \\
 S_3 &= K_3 \cdot f \cdot R_{total} \cdot R_{total} \cdot L \\
 S_4 &= K_4 \cdot f \cdot R_{pinch} \cdot R_{pinch} \cdot L
 \end{aligned}
 \tag{2}$$

where K<sub>1</sub>, K<sub>2</sub>, K<sub>3</sub>, K<sub>4</sub>, f, and L indicate the coefficients, the frequency of the short circuit mode, and the droplet length, respectively.

In order to calculate the parameters, the motion of the droplet volume should

be simulated. It is governed by the continuity equation and the momentum equation,

$$\nabla \cdot v = 0 \tag{3}$$

$$\frac{\partial v}{\partial t} + (v \cdot \nabla)v = -\frac{1}{\rho} \nabla P + \nu \nabla^2 v + \frac{F}{\rho} \tag{4}$$

where ρ, ν, and F denote the mass density, the kinematic viscosity, and the body force, respectively. The body force includes the electromagnetic force as well as gravity. These equations were solved using the volume of fluid (VOF) method, because this technique has advantages of numerical stability and efficiency in algorithms. The detailed mathematical descriptions of Equations 3, 4, and VOF are given elsewhere (Ref. 17).

The droplet volume, the arc current, and the short circuit current were used as the conditions for the simulations. The droplet volume was calculated by means of dividing the wire feed rate by the fre-

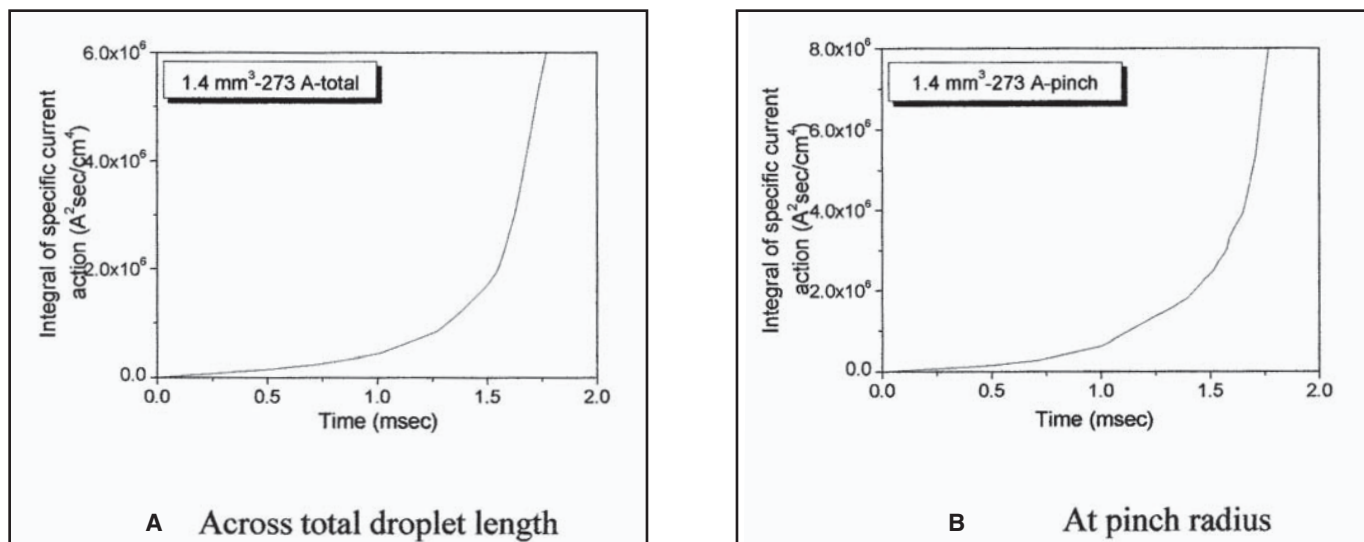


Fig. 4 — Integral of specific current action at the short circuit time for Condition 1 in Table 3.

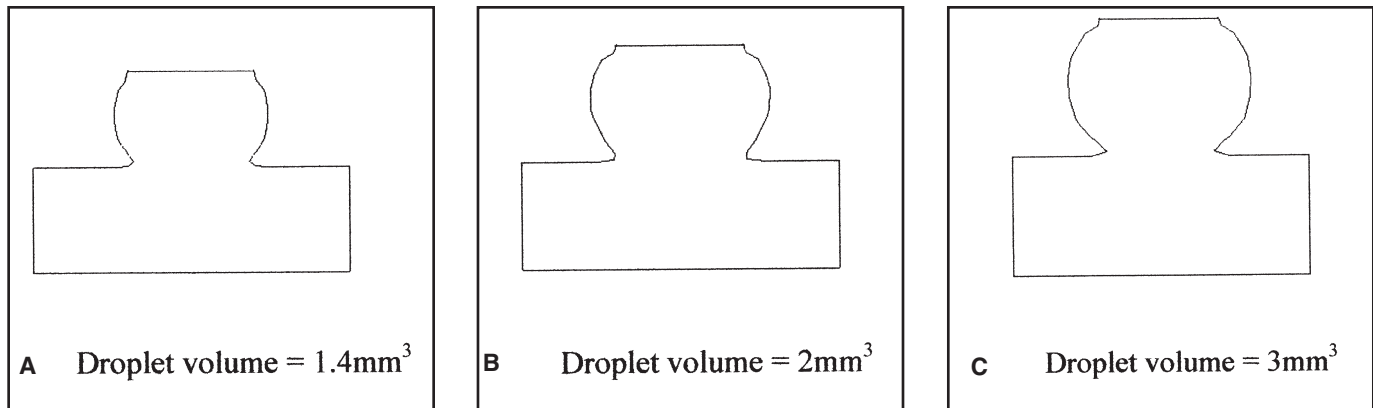


Fig. 6 — Shape of droplet and molten pool at the short circuit beginning.

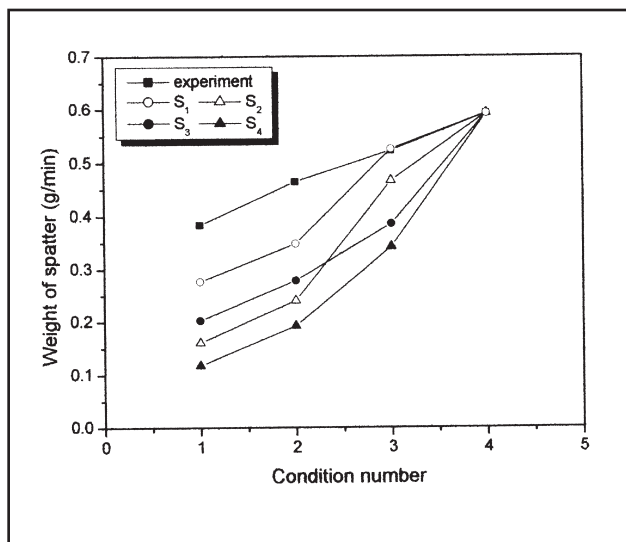


Fig. 7 — Comparison of the spatter calculations with the welding experiments for the conditions in Table 3.

ulations were carried out for a steel electrode with a 1.2-mm diameter. The material properties used for the calculations are listed in Table 2.

## Results and Discussions

### The Constant Value of the Integral of Specific Current Action

In order to check whether the value of  $h$  from previous papers can be used as a constant value in this study, the welding conditions with typical waveforms of the short circuit mode and different spatter productions were chosen, as listed in Table 3.

Conditions 1 and 2 had an arc current of 175 A, while conditions 3 and 4 had 223 A. With these currents, the values of  $h$  at the arc time were calculated and are displayed in Figure 3. The value of  $h$  is proportional to time, which is apparent from Equation 1, as shown in Fig. 3. When Fig. 3A is compared with Fig. 3B, the value of

$h$  at 223 A is larger than that of 175 A at the same amount of time, because the current density at 223 A is higher than that of 175 A.

Conditions 1–4 have 273 A, 320 A, 299 A, and 345 A as their peak currents, respectively. The values of  $h$  at the short circuit time were calculated for all conditions, and the two values of  $h$  in condition 1 are presented in Fig. 4. This shows that, due to the small pinch radius, the two values of  $h$  increased drastically as the short circuit time increased.

The summation of the values of  $h$  for the arc

time and the short circuit time for the conditions in Table 3 are compared with the value of  $h$  with the order of  $10^7 \text{ A}^2\text{s}/\text{cm}^4$  from the previous papers. The value of  $h$  in this study was found to have the order of  $10^6 \text{ A}^2\text{s}/\text{cm}^4$ , which shows that the value of  $h$  from previous papers is not applicable in this study. Based on the calculated results of conditions 1 to 4, the value  $5 \times 10^6 \text{ A}^2\text{s}/\text{cm}^4$  was chosen for the constant value of  $h$ , because it was the smallest value of conditions 1 to 4.

Bukarov and Ermakov found that the radius at the short circuit breakage was between approximately 0.2 and 0.4 mm (Ref. 16). From trial simulations, it was revealed that condition 1 made the smallest pinch radius, while condition 4 made the largest. Consequently, it was assumed that the 0.2-mm radius was formed in condition 1 and the 0.4-mm radius was formed in condition 4. Based on these assumptions, the values of  $h$  were calculated and are presented in Table 4. The values are around

Table 4 — Integral of Specific Current Action for its Verification

	At pinch radius	Across total droplet length
Condition 1	$3.59 \times 10^6 \text{ A}^2\text{s}/\text{cm}^4$	$2.89 \times 10^6 \text{ A}^2\text{s}/\text{cm}^4$
Condition 4	$4.47 \times 10^6 \text{ A}^2\text{s}/\text{cm}^4$	$4.19 \times 10^6 \text{ A}^2\text{s}/\text{cm}^4$

Table 5 — Pinch Radius Calculated by Using the H-value,  $5 \times 10^6 \text{ A}^2\text{s}/\text{cm}^4$

Condition number	$R_{\text{total}}$ (mm)	$R_{\text{pinch}}$ (mm)
1	0.119	0.131
2	0.164	0.197
3	0.136	0.185
4	0.207	0.299

Table 6 — Droplet Length Calculated for the Conditions in Table 3

Condition number	Droplet volume ( $\text{mm}^3$ )	Droplet length (mm)
1	1.4	1.1
2	2.0	1.2
3	1.4	1.1
4	3.0	1.5

$10^6 \text{ A}^2\text{s}/\text{cm}^4$ , which validates that  $5 \times 10^6 \text{ A}^2\text{s}/\text{cm}^4$  is acceptable for the constant value of  $h$ .

quency of the short circuit mode. The arc current and the short circuit current were measured in the welding experiments.

## Welding Experiments

This study focused on spatter production in the short circuit mode. Therefore, the welding experiments were carried out in the conditions of the short circuit mode. They were conducted four times for one condition using four different welding machines. The welding current and voltage were used as set variables, and the welding current was measured with a Hall-effect sensor attached to the ground cable, while the arc voltage was measured from the output terminals of the welding power source. The measured signals were put into a computer through an A/D converter with a sampling rate of 10 kHz. The typical waveforms and parameters are shown in Fig. 1. A collecting box was made from brass and used to prevent the spatter production from spreading out. The spatter in the collecting box was subsequently gathered and screened using a sieve. Certain characteristics of the spatter, such as the type of size, were not considered. The spatter production was weighed with an electric scale. Other welding variables are listed in Table 1.

## Simulation Technique

The boundary conditions at the arc time and the short circuit time were imposed as shown in Fig. 2. At the arc time, the initial droplet shape was assumed to be a hemisphere to ensure numerical stability, and the free slip condition was enforced along the z axis. At the short circuit time, the initial droplet was assumed to be spherical and to touch the molten pool with a contact diameter of 1.2 mm, in order to ensure numerical stability. The free slip condition was established along the z axis, as well as on the boundary surface of the molten pool. At the arc time, the current density was assumed to be uniform on the surface of the droplet, while it was assumed to be uniform on the boundary surface of the molten pool at the short circuit time. Detailed descriptions of the procedure to obtain the current density are given elsewhere (Refs. 17, 18).

A square cell of 0.1 mm, which has been used in previous works and resulted in acceptable simulations, was used for the simulations in this study (Ref. 17). At the arc time, the dimension of solution domain was 3 and 10 mm in the r and z directions, respectively, while it was 4 mm in both directions for the droplet volume at  $< 2 \text{ mm}^3$ , and 4 and 5 mm in the r and z directions, respectively, for the droplet volume  $\geq 2 \text{ mm}^3$  at the short circuit time. The sim-

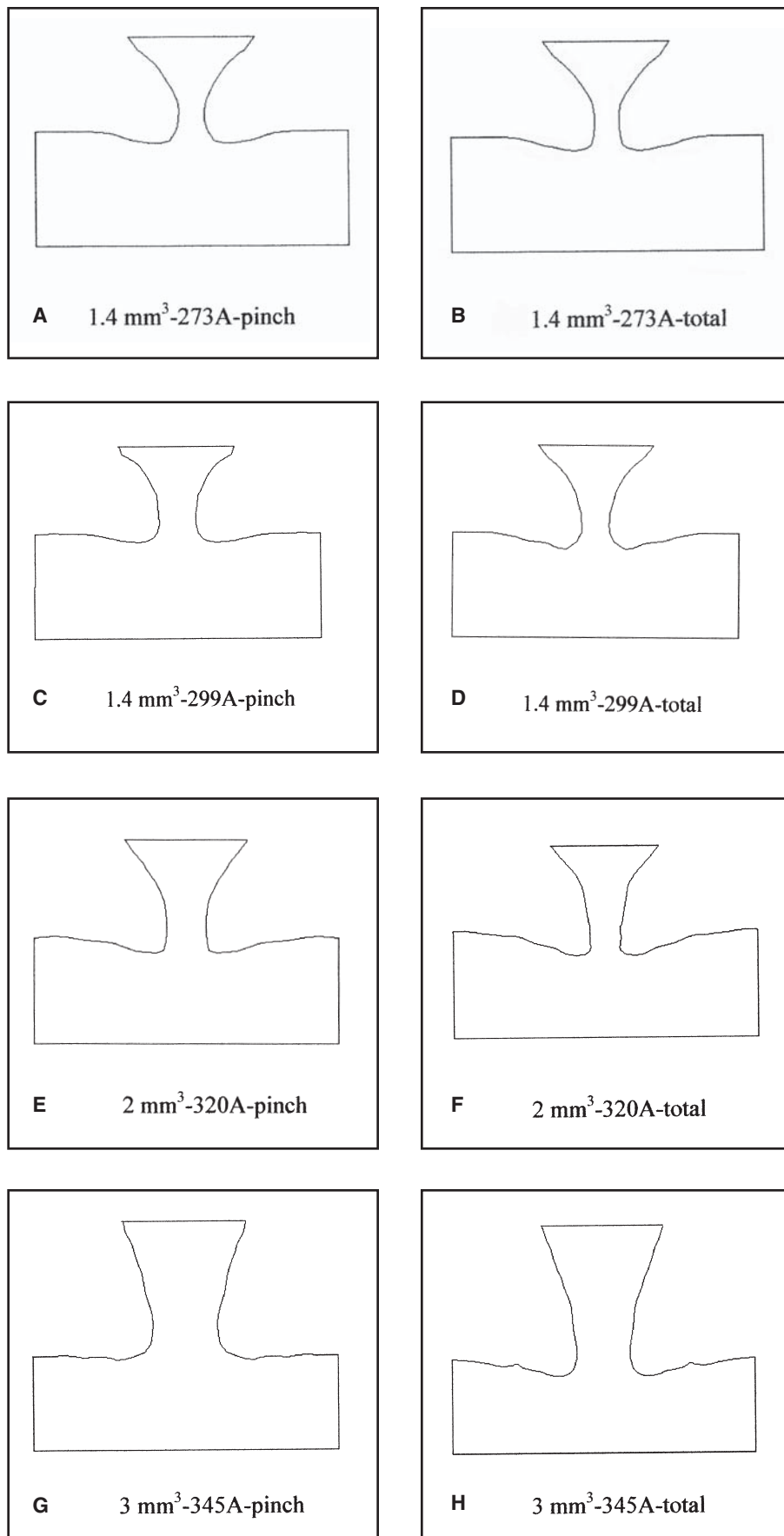


Fig. 5 — Shape of the droplet and molten pool at the integral of specific current action,  $5 \times 10^6 \text{ A}^2\text{s/cm}^4$ .

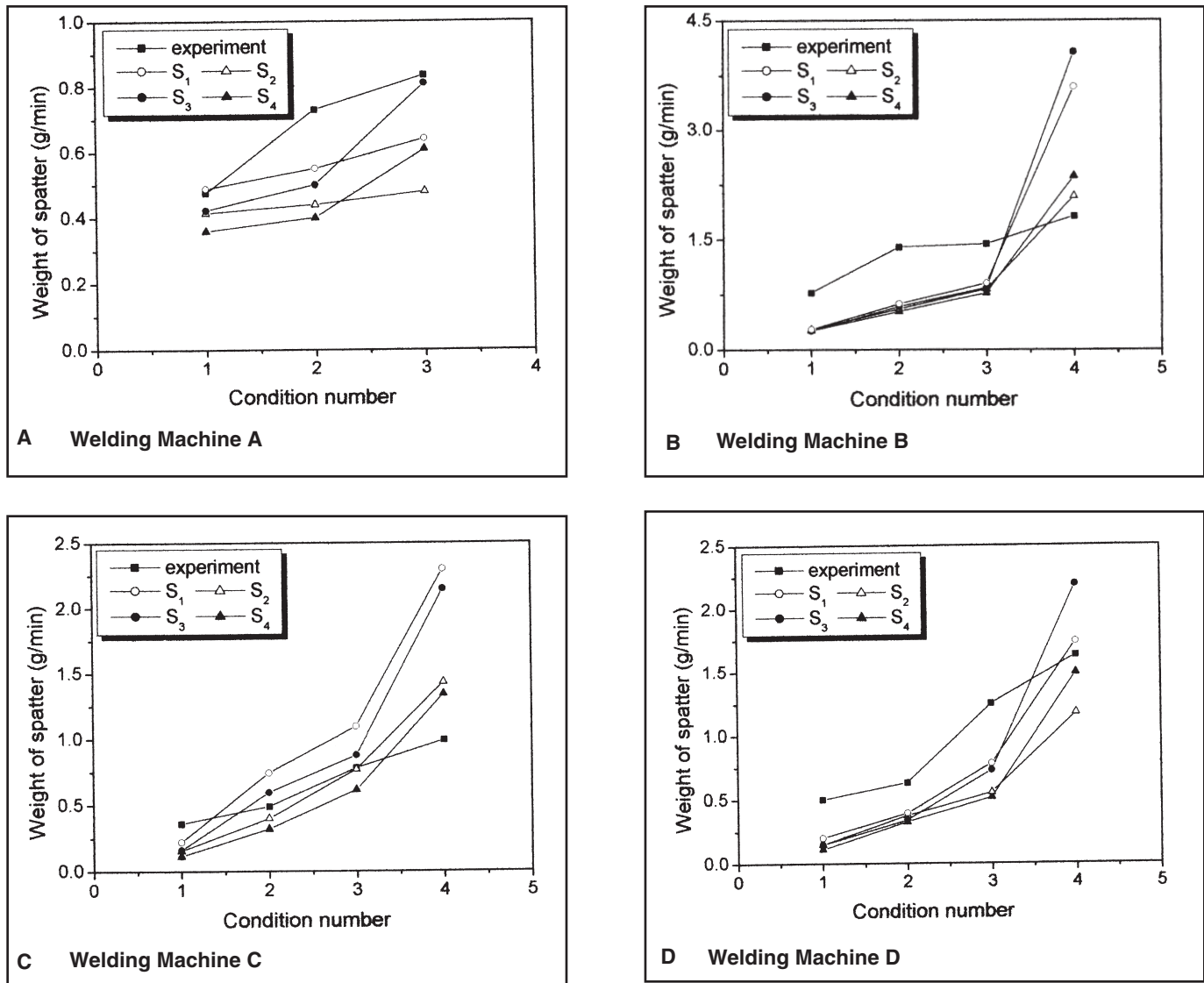


Fig. 8 — Comparison of the spatter calculations with the welding experiments for four different welding machines.

### Spatter Calculation

For the conditions in Table 3, the pinch radius, the droplet length, and the frequency of the short circuit mode are calculated and presented in Tables 5 and 6.

The  $h$ -value of  $R_{pinch}$  was calculated at the pinch radius, the smallest radius, while the  $h$ -value of  $R_{total}$  was calculated across the total droplet length, where the radius is larger than that of the pinch radius. Consequently, the  $h$ -value of  $R_{pinch}$  reaches the constant value,  $5 \times 10^6$   $A^2s/cm^4$ , earlier than that of  $R_{total}$ ;  $R_{pinch}$  also becomes larger than  $R_{total}$  due to the decreased time. This fact can also be found in Fig. 4. Related to the pinch radius, the shapes of the droplet and molten pool calculated at the moment of  $5 \times 10^6$   $A^2s/cm^4$  are shown in Fig. 5.

The droplet length increases as the droplet volume increases, as shown in Fig. 6. The droplet length for the droplet vol-

ume of  $3 \text{ mm}^3$  is 1.5 mm, which is larger than the length of 1.1 mm calculated for droplet volume of  $1.4 \text{ mm}^3$ .

A large arc voltage has enough time to shape a larger droplet volume due to the long arc, when compared to a small voltage at the same wire feed rate (Refs. 17, 20). The droplet volume multiplied with the frequency is constant due to the same wire feed rate, which causes the frequency to decrease as the droplet volume increases. This explains that the frequency of the short circuit mode decreases from 48.8 to 32.3 Hz at a wire feed rate of 60 mm/s, and from 70.9 to 34.5 Hz at a wire feed rate of 91 mm/s when the arc voltage increases, as shown in Table 7.

In order to calibrate  $K_1$ ,  $K_2$ ,  $K_3$ , and  $K_4$  from Equation 2, condition 4 in Table 3 was used. Then, the spatter production was calculated for the remaining conditions in Table 3 and presented in Fig. 7. It can be seen that  $S_1$ ,  $S_2$ ,  $S_3$ , and  $S_4$  followed

Table 7 — Frequency of Short Circuit Mode Calculated for the Conditions in Table 3

Condition number	Frequency (Hz)
1	48.8
2	32.3
3	70.9
4	34.5

the trends of the welding experiments appropriately. The spatter production from condition 4 was more than that of condition 1, as shown in Fig. 7. Condition 4 had a larger pinch radius and droplet length, while condition 1 had a higher frequency. This shows that spatter production is affected by various parameters.

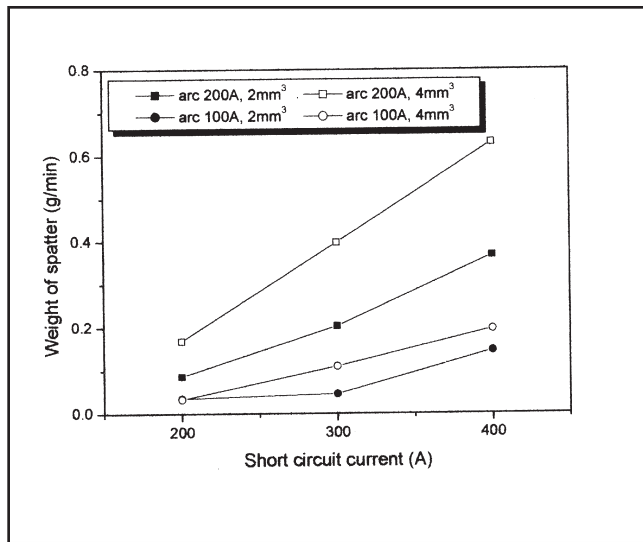


Fig. 9 — Spatter calculations vs. short circuit current for the four conditions of arc current and droplet volume.

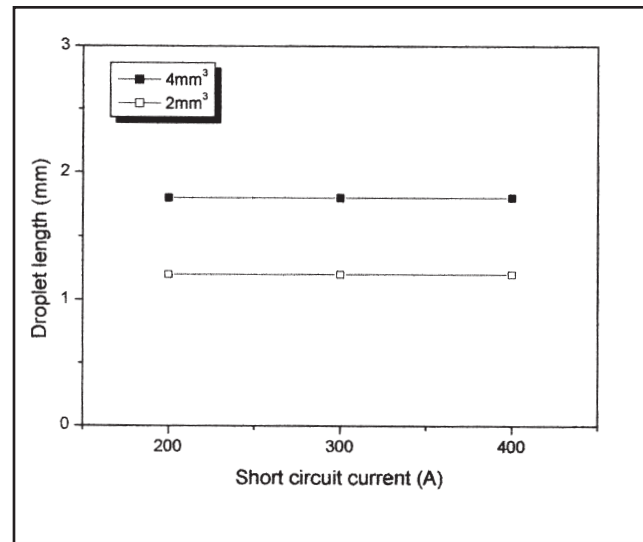


Fig. 10 — Calculated droplet length vs. short circuit current for two droplet volumes.

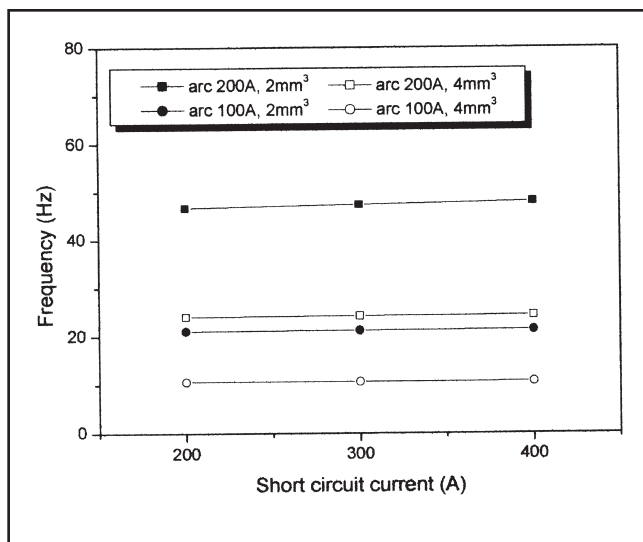


Fig. 11 — Calculated frequency of short circuit mode vs. short circuit current for the four conditions of arc current and droplet volume.

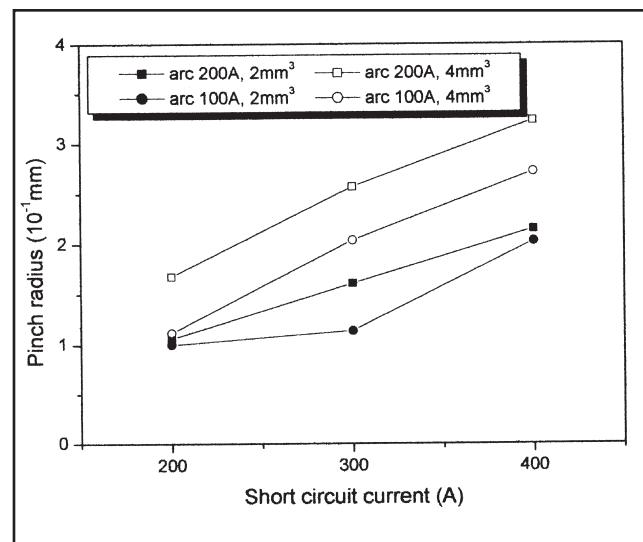


Fig. 12 — Calculated pinch radius vs. short circuit current for the four conditions of arc current and droplet volume.

Table 8 — Welding Conditions of the Four Different Welding Machines

	A	B	C	D
1	60 mm/s, 19.8 V	65.4 mm/s, 17.5 V	51.6 mm/s, 20.8 V	19.2 mm/s, 17.2 V
2	91 mm/s, 15.8 V	91.8 mm/s, 17.0 V	82.8 mm/s, 20.1 V	28.8 mm/s, 17.8 V
3	91 mm/s, 17.9 V	127.2 mm/s, 16.7 V	111.6 mm/s, 21.0 V	28.8 mm/s, 18.9 V
4		127.2 mm/s, 18.9 V	111.6 mm/s, 23.2 V	47.4 mm/s, 19.2 V

To generalize Equation 2, the spatter calculations were conducted with four dif-

ferent welding machines for the welding conditions listed in Table 8; following the

previous procedure, the spatter production is calculated and presented in Fig. 8.

For the performance analysis of  $S_1$ ,  $S_2$ ,  $S_3$ , and  $S_4$ , the correlation coefficients were calculated and are listed in Table 9. The values of  $S_2$ ,  $S_3$ , and  $S_4$  are all approximately 0.8, while that of  $S_1$  is nearly 0.7. This shows that the four methods are acceptable. The values of  $S_2$  and  $S_4$ , calculated with  $R_{pinch}$ , are higher than those of  $S_1$  and  $S_3$ , calculated with  $R_{total}$ . The value of  $S_4$ , calculated with the droplet length, is higher than that of  $S_2$ , calculated without the droplet length. This is most likely due to the fact that spatter production occurs at the weakest location, such as the pinch radius, and the droplet length influences the volume of the short circuit bridge.

The modeling of spatter formation is

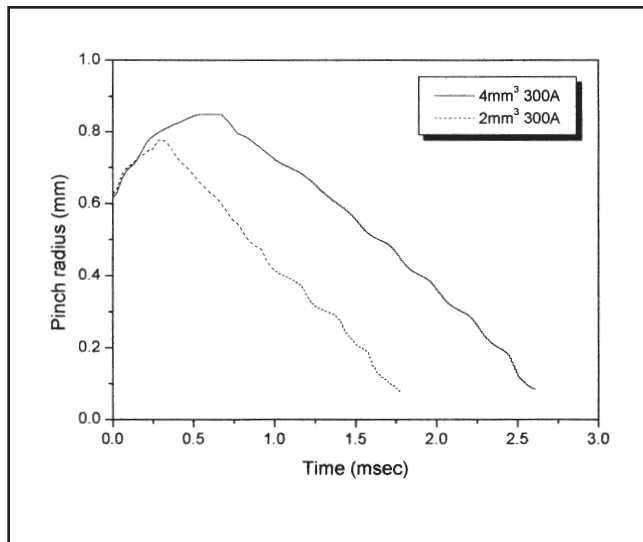


Fig. 13 — Time history of calculated pinch radius for two droplet volumes.

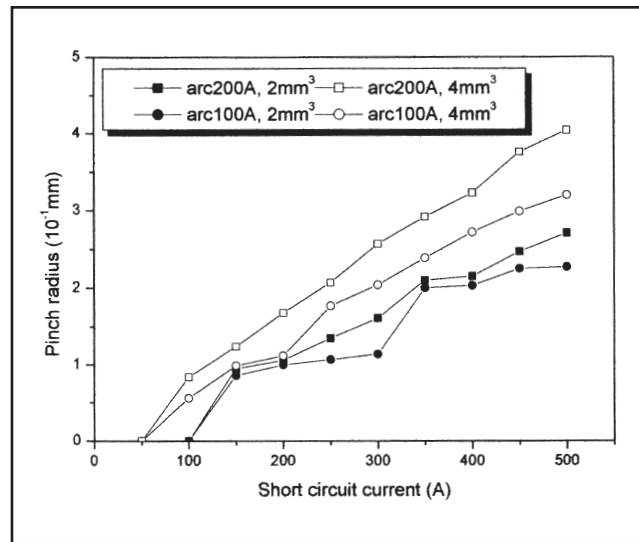


Fig. 14 — Variation of pinch radius as the short circuit current changes.

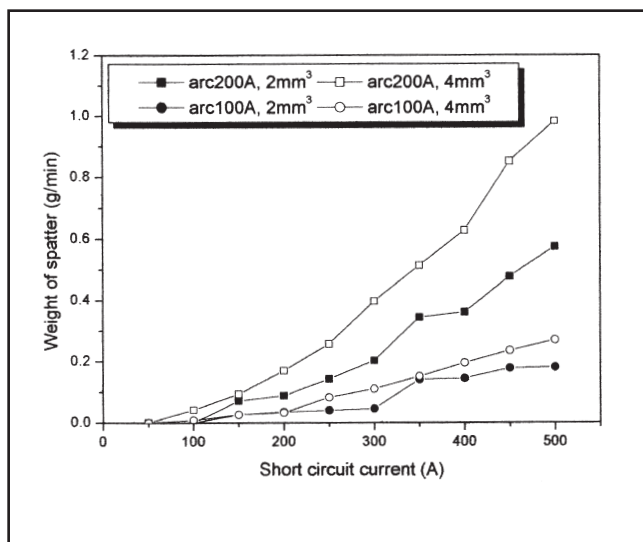


Fig. 15 — Variation of spatter generation as the short circuit current changes.

difficult work since spatter generation is related with complicated physical phenomena, which are not known clearly. Particularly at the moment of the short circuit breakage, the influence of pinch radius, arc length, and frequency on spatter is difficult to test. It causes errors of  $S_1$ ,  $S_2$ ,  $S_3$ , and  $S_4$  between simulations and experiments. This may be an area for future improvement.

### Influence of Parameters on Spatter Production

From previous studies, the peak current and arc time are found to have a strong correlation with spatter production (Refs. 2–5), but they do not illustrate how these parameters affect spatter production. In the previous section, the param-

eters change concurrently, which makes it difficult to investigate their influence separately. For this analysis, two conditions of arc current, two conditions of droplet volume, and three conditions of short circuit current were chosen, as shown in Table 10.

The procedure of the simulations follows that outlined in the previous section, and the results are shown in Figs. 9–12. The spatter production was calculated by way of  $S_4$ , because it had the highest correlation coefficient.

$S_4$  increased from 0.17 to 0.63 g/min when the droplet volume and arc current were fixed at 4 mm<sup>3</sup> and 200 A, respectively, and the short circuit current increased from 200 to 400 A, as shown in Fig. 9. The droplet volume determines the droplet length and, consequently, the droplet length does not change in this case. A large short circuit current reaches the constant h-value of  $5 \times 10^6$  A<sup>2</sup>/cm<sup>4</sup> earlier than the small one due to the large current density. This decreases the short circuit time and the pinch radius increases, as shown in Fig. 12. The short circuit time is relatively small when compared with the arc time dominant to determine the frequency. Therefore, the change of frequency is tiny, although the short circuit time is enormous. Consequently, the increase in spatter production is due to the increased pinch radius. This

Table 9 — Correlation Coefficients for the Four Ways to Calculate the Spatter Production

	Correlation coefficient
$S_1$	0.722
$S_2$	0.780
$S_3$	0.757
$S_4$	0.809

Table 10 — Simulation Conditions for the Investigation of the Influence of Droplet Volume, Arc Current, and Short Circuit Current on Spatter Production

Droplet volume	2 mm <sup>3</sup> , 4 mm <sup>3</sup>
Arc current	100 A, 200 A
Short circuit current	200 A, 300 A, 400 A

explains the role of the peak current in spatter production because it is similar to that of the short circuit current.

Figure 9 shows that the  $S_4$ , calculated for the droplet volume of 4 mm<sup>3</sup> (case 1), was approximately 0.26 g/min larger than the  $S_4$ , calculated for the droplet volume of 2 mm<sup>3</sup> (case 2), when the arc current and short circuit current were kept at 200 and 400 A, respectively. The droplet length in case 1 became larger than that of case 2 due to the larger droplet volume, as shown in Fig. 10. The short circuit frequency became proportional to the reciprocal of the droplet volume, which resulted in 24.4 Hz for case 1 and 48.1 Hz for case 2. This means that the time to shape the droplet in case 1 is twice

as long as that of case 2 during this arc time. This yields a higher  $h$ -value at the arc time and a larger pinch radius in case 1, which remains large for a long time, before the value of  $h$  reaches  $5 \times 10^6 \text{ A}^2/\text{cm}^4$ , as seen in Fig. 13. Figure 12 shows that the pinch radius in case 1 is 0.323 mm and larger than the 0.215 mm of case 2. Consequently, the increased droplet length and pinch radius of case 1 resulted in a larger spatter production than that of case 2, although the frequency was smaller. This result explains the role of arc time in spatter production, because arc time is proportional to droplet volume.

It is observed that the  $S_4$  calculated for the arc current of 200 A (case 3) is about 0.43 g/min larger than the  $S_4$  calculated for the arc current of 100 A (case 4), when the droplet volume and the short circuit current are kept at  $4 \text{ mm}^3$  and 400 A, respectively, as shown in Fig. 9. These two cases have the same droplet length due to the same droplet volume, while the wire feed rate in case 3 is approximately twice that of case 4. This results in 24.4 Hz for case 3, which is nearly twice that of the 10.7 Hz for case 4, as shown in Fig. 11. The arc time to form the droplet in case 4 becomes roughly twice as long as that of case 3, because the wire feed rate of case 3 was about double that of case 4. Using Equation 1 results in the  $h$ -value of case 3 being twice as high as that of case 4, which causes the time required to reach the constant  $h$ -value of  $5 \times 10^6 \text{ A}^2/\text{cm}^4$  to be larger in case 4 than in case 3 during the short circuit time. The pinch radius was calculated to be 0.27 mm in case 4, while case 3 was 0.32 mm. The increase in spatter production in case 3 is certainly due to the increased frequency and pinch radius. This may explain the effect of the wire feed rate on spatter production, because the arc current is proportional to the wire feed rate.

It is useful to investigate how spatter production changes with the pinch radius at the short circuit breakage as the short circuit current increases. For this analysis, the short circuit current was made to change from 50 to 500 A, while the arc current and droplet volume in the previous section were used. The calculated pinch radius is shown in Fig. 14. The pinch radius of the droplet volume of  $4 \text{ mm}^3$  increases more linearly than that of  $2 \text{ mm}^3$ . The top side of the droplet volume in simulations is fixed with 1.2 mm because it is in contact with the solid part of the electrode as shown in Fig. 5. It influences the variation of free surface profiles of droplet and weld pool. Its effect becomes large if the droplet length is short. The droplet length of  $2 \text{ mm}^3$  is 1.2 mm, which is shorter than that of  $4 \text{ mm}^3$ . Due to this, the non-linear change of the pinch radius at the condition of  $2 \text{ mm}^3$  is thought to occur.

With the data of Fig. 14, spatter production was calculated and is shown in Fig.

15.  $S_4$  is the quadratic equation of  $R_{\text{pinch}}$  as shown in Equation 2.  $S_4$  at the condition of the arc current of 200 A and the droplet volume of  $4 \text{ mm}^3$  shows the characteristic of quadratic increase clearly. The pinch radius rises linearly in proportion to the short circuit current as shown in Fig. 14. It causes spatter generation to be on the quadratic increase as the short circuit current grows. At the other conditions, except that of the arc current of 200 A and the droplet volume of  $4 \text{ mm}^3$ , the pinch radius is not on the linear increase as the short circuit current changes. Therefore, quadratic change is not shown clearly.

## Conclusions

The integral of the specific current action is introduced to quantitatively explain the mechanism of spatter production. Based on previous studies, it was proposed that there is a constant value for the integral of a specific current action to determine the moment of the short circuit breakage. A constant value of  $5 \times 10^6 \text{ A}^2/\text{cm}^4$  was found to be appropriate, using simulations, and used to calculate the pinch radius. The frequency of the short circuit mode and the droplet length were calculated from the welding experiments and simulations. By using these parameters, four ways of calculating spatter production were proposed. The correlation coefficients of the proposed four ways show that they are all acceptable.

The influence of droplet volume, arc current, and short circuit current on spatter production was investigated quantitatively. The droplet volume changed the frequency, the droplet length, and the pinch radius, which explained the role of the arc time in spatter production. The short circuit current varies the current density, which determines the pinch radius, and consequently affects spatter production. This illustrates the role of the peak current in spatter production and provides a basis for the control of spatter production by changing the peak current during the short circuit time. The arc current influences the frequency and current density, which causes a change in spatter production, too.

The pinch radius at the short circuit breakage in the condition of large droplet volume is on the linear increase, resulting in the quadratic increase of spatter production, as the short circuit current rises.

## References

- Chen, J. H., Sun, Z. C., and Fan, D. 1996. Study on the mechanism of spatter produced by basic welding electrodes. *Welding Journal* 75(10): 312-s to 316-s.
- Mita, T., Sakabe, A., and Yokoo, T. 1988. Quantitative estimates of arc stability for  $\text{CO}_2$  gas shielded arc welding. *Welding International*

2(2): 152–159.

3. Kang, M. J., and Rhee, S. 2001. The statistical models for estimating the spatter rate in the short circuit transfer mode of GMAW. *Welding Journal* 80(1): 1-s to 8-s.

4. Kang, M. J., Kim, Y., Ahn, S., and Rhee, S. 2003. Spatter rate estimation in the short-circuit transfer region of GMAW. *Welding Journal* 82(9): 238-s to 247-s.

5. Lipei, J. 1988. The effect of the dynamic behavior of welding rectifiers on spatter. *Welding International* 2(3): 263–268.

6. Yamanoto, H., Harada, S., and Yasuda, T. 1990. The development of welding current control systems for spatter reduction. *Welding International* 4(5): 398–407.

7. Mita, T. 1989. Reducing spatter in  $\text{CO}_2$  gas shielded arc welding — waveform control. *Welding International* 3(3): 227–232.

8. Maruyama, T., Sato, M., and Hida, Y. 1990. Waveform control in gas shielded arc welding. *Welding International* 4(9): 677–683.

9. Ueguri, S., Hara, K., and Komura, H. 1985. Study of metal transfer in pulsed GMA welding. *Welding Journal* 64(8): 242-s to 250-s.

10. Ito, T., Koshiishi, F., Sato, M., Suga, T., and Ushio, M. 1998. Study of spatter reduction in pulsed  $\text{CO}_2$  shielded arc welding. *Welding International* 12(5): 366–371.

11. Valentin, S. S., Gennady, A. M., Vladimr, I. O., Vladimir, V. V., and Lyudmila, I. C. Au. 1999. The current density and the specific energy input in fast electrical explosion. *IEEE Transactions on Plasma Science* 27(4): 845–850.

12. Gennady, A. M. De. 1995. Ecton mechanism of the vacuum arc cathod spot. *IEEE Transactions on Plasma Science* 23(6): 879–883.

13. Chace, W. G., and Moore, H. K. 1968. *Exploding wire*. New York: Plenum Press, pp. 1–25.

14. Chace, W. G., and Moore, H. K. 1959. *Exploding wire*. New York: Plenum Press, pp. 97–103.

15. Mita, T. 1991. Spatter reduction - power source considerations. *Welding International* 5(11): 847–850.

16. Bukarov, V. A., and Ermakov, S. S. 1993. Dynamics of energy characteristics of the arc in consumable electrode short-circuit welding. *Welding International* 7(2): 129–133.

17. Choi, S. K., Yoo, C. D., and Kim, Y. S. 1998. Dynamic simulation of metal transfer in GMAW, part 1: Globular and spray transfer modes. *Welding Journal* 77(1): 38-s to 44-s.

18. Choi, S. K., Ko, S. H., Yoo, C. D., and Kim, Y. S. 1998. Dynamic simulation of metal transfer in GMAW, part 2: Short circuit transfer mode. *Welding Journal* 77(1): 45-s to 51-s.

19. Chace, W. G., and Moore, H. K. 1964. *Exploding Wire*. New York: Plenum Press, pp. 295–313.

20. Choi, J. H., Lee, J. Y., and Yoo, C. D. 2001. Simulation of dynamic behavior in a GMAW system. *Welding Journal* 80(10): 239-s to 245-s.